Search for $ZW + ZZ \to \ell^+\ell^-+$ jets production in $p\bar{p}$ collisions at $\sqrt{s} = 1.96$ TeV

The CDF Collaboration[1]

[1] *http://www-cdf.fnal.gov*

(Dated: February 22, 2012)

Abstract

We present a measurement of the cross section of ZW and ZZ production in the dilepton + dijet final state using 8.9 fb^{-1} of data recorded with the CDF detector at the Tevatron. We increase our sensitivity to $W/Z \to q\bar{q}'$ decays using a quark-gluon neural network discriminant that quantizes the spatial spread of the energy and track momenta contained within a jet. Additionally, we employ new jet energy corrections to Monte Carlo simulations that account for differences in the energy scale of quark and gluon jets. The number of signal events is extracted through a simultaneous fit to the dijet mass spectrum in three channels: a heavy-flavor tagged channel, a light-flavor tagged channel, and an untagged channel. We measure $\sigma_{ZW/ZZ} = 2.5^{+2.0}_{-1.0}$ pb, consistent with the standard model prediction of 5.1 pb. We establish an upper limit on the cross section of $\sigma_{ZW/ZZ} < 6.1$ pb at 95% confidence level.

I. INTRODUCTION

The standard model (SM) offers precise predictions for the production rates for self-interactions of the gauge bosons [1]. Differences between these predictions and measured diboson production cross sections may indicate the presence of new physics [2, 3], perhaps specifically in hadronic final states [4]. Additionally, since hadronic final states in diboson production are similar to associated Higgs boson production ($p\bar{p} \to VH+X$ where V=W, Z), the analysis techniques used to measure diboson production in partially hadronic final states are relevant to Higgs boson searches.

Experiments at the Tevatron have previously measured the production of two gauge bosons in partially hadronic decay channels [5–8], but each of these measurements have included sensitivity to WW production, which has a higher cross section than ZW and ZZ production. Searches using b-tagging to increase sensitivity to events with $Z \to b\bar{b}$ decays have been conducted [9], but have not yet observed ZW/ZZ production in partially hadronic decay channels.

We present a measurement of the cross section of ZW/ZZ production in a final state with two leptons and at least two jets. We require the two leptons to be from the decay of a Z boson, and search for associated $W/Z \to q\bar{q}'$ decays by performing a fit to the dijet invariant mass (m_{jj}) spectrum of the two leading E_T jets. To maximize our sensitivity to diboson production, we separate events into three channels: a heavy-flavor tagged channel, largely sensitive to $ZZ \to \ell^+\ell^- b\bar{b}$ decays; a light-flavor tagged channel which utilizes a new artificial neural-network-based discriminant that separates quark jets from gluon jets; and an "untagged" channel which contains the remaining events that pass our event selection requirements. The fit to the m_{jj} spectrum is performed simultaneously across these three channels.

II. THE CDF DETECTOR

The CDF II detector is described in detail elsewhere [10]. The detector is cylindrically symmetric around the proton beam line [11]. Tracking detectors are installed around the interaction point, and reconstruct the trajectories of charged particles. The tracking systems sit within a superconducting solenoid which produces a 1.4 T magnetic field aligned coaxially

with the $p\overline{p}$ beams. Around the outside of the solenoid, calorimeter modules arranged in a projective tower geometry measure the energies of charged and neutral particles. A series of drift chambers sit outside the calorimeter, and are used to detect muons, which typically leave little energy in the calorimeter.

The Central Outer Tracker (COT) is a 3.1 m long open cell drift chamber which performs 96 track measurements in the region between 0.40 and 1.37 m from the beam axis, providing coverage in the pseudorapidity region $|\eta| \leq 1.0$. Sense wires are arranged in eight alternating axial and $\pm$ 2° stereo "superlayers" with 12 wires each. The position resolution of a single drift time measurement is about 140 μm. A five-layer double-sided silicon microstrip detector (SVX) covers the region between 2.5 to 11 cm from the beam axis. Three separate SVX barrel modules along the beam line cover a length of 96 cm, approximately 90% of the luminous beam interaction region. Three of the five layers combine an r-ϕ measurement on one side and a 90° stereo measurement on the other, and the remaining two layers combine an r-ϕ measurement with a small angle ($\pm$1.2°) stereo measurement. The typical silicon hit resolution is 11 μm. Additional Intermediate Silicon Layers (ISL) at radii between 19 and 30 cm from the beam line in the central region link tracks in the COT to hits in the SVX. The fiducial range of the silicon detector extends to $|\eta| \leq 2.0$.

Calorimeter modules sit outside the central tracking volume and solenoid. The inner electromagnetic layers consists of lead sheets interspersed with scintillator, while the outer hadronic layers consist of scintillators sandwiched between steel sheets. The calorimeter is split between central barrel ($|\eta| \leq 1.0$) and forward end plug ($1.1 \leq |\eta| \leq 3.6$) sections. Individual towers in central barrel subtend 0.1 in $|\eta|$ and 15° in ϕ. The sizes of the towers in the end plug calorimeter vary with $|\eta|$: subtending 0.1 in $|\eta|$ and 7.5° in ϕ at $|\eta| = 1.1$, and 0.5 in $|\eta|$ and 15° in ϕ at $|\eta| = 3.6$.

High-momentum jets, photons, and electrons leave isolated energy deposits in contiguous groups of calorimeter towers which can be summed together into an energy cluster. Electrons are identified as isolated, mostly electromagnetic clusters, and quality cuts may be placed on the presence of a high-p_T track matched to the cluster. Jets are identified as electromagnetic and hadronic clusters with an electromagnetic fraction $\frac{E_{EM}}{E_{total}} = \frac{E_{EM}}{E_{EM}+E_{had}} \leq 0.9$, clustered using the JETCLU cone algorithm [12] with a fixed cone size of $\Delta R \equiv \sqrt{(\Delta\eta)^2 + (\Delta\phi)^2} = 0.4$.

Outside the calorimeters, a collection of drift chambers detect muons. A four-layer stack of planar drift chamber detects muons with $p_T > 1.4$ GeV/c, and another four layers of drift

chambers behind 60 cm of steel detects muons with $p_T > 2.0$ GeV/c. Both systems cover a region of $|\eta| \leq 0.6$, though they have different structure and their geometrical coverages do not overlap exactly. Muons in the region between $0.6 \leq |\eta| \leq 1.0$ pass through at least four drift layers lying in a conic section outside of the central calorimeter. Muons may be identified as either COT tracks that extrapolate to hits on the muon detectors, or isolated tracks unmatched to hits in the muon detectors, but with tighter tracking quality requirements.

III. DATASET AND EVENT SELECTION

We analyze the full dataset of $p\overline{p}$ collisions collected by the CDF II detector. We require events to be from periods where the calorimeter, muon detectors, and silicon detectors were all functioning properly, corresponding to an integrated luminosity of 8.9 fb^{-1}. Events are selected via a suite of high-E_T electron and high-p_T muon triggers, the bulk of which require at least one lepton with $E_T/p_T > 18$ GeV/c. We require events contain two electrons or two muons with $E_T/p_T \geq 20$ GeV/c, and we calculate the trigger and reconstruction efficiencies by comparing the number of data and simulated $Z \to \ell\ell$ events with exactly one jet with $E_T > 20$ GeV.

For the final analysis, we select events with two leptons, and two or more jets. In addition to the p_T requirements on the leptons, we require leptons with well-reconstructed tracks (central electrons and all muons) to be of opposite charge, and that the reconstructed dilepton invariant mass, $m_{\ell\ell}$, be consistent with the mass of the Z boson: 76 GeV/c^2 $\leq$ $m_{\ell\ell} \leq$ 106 GeV/c^2. We require both leading-E_T jets have $E_T > 25$ GeV and $|\eta| \leq 2.0$, and not be matched within $\Delta R \leq 0.4$ to a reconstructed lepton. Additionally, the two jets must be separated with $\Delta R \geq 0.7$. Finally, as our final state should contain no objects that fail to be reconstructed in the detector, we also require the missing transverse energy, $\not\!\!E_T$ [13], be less than 20 GeV.

After this selection, we have three major sources of background. Our dominant background comes from production of a Z boson which decays to an e^+e^- or $\mu^+\mu^-$ pair, produced in association with two jets. Simulated events generated using ALPGEN [14] interfaced with PYTHIA [15] for showering are used to estimate this background. The contributions from $Z + b\bar{b}$ processes are enhanced, in order to agree with measurements [16].

Another significant background results from jets misidentified as leptons. The contributions from these lepton "fakes" are estimated using data-driven methods. For muons, we use events with same-sign muon pairs (rather than opposite-sign) that otherwise satisfy all of our event selection requirements. For electrons, we construct a misidentification rate representing the likelihood a jet is misidentified as an electron, as a function of jet E_T and η using jet-triggered data that have few electrons. This rate is then applied to e-jet pairs in the high-p_T electron dataset, where the jet is then treated as a second electron, and the event selection requirements are otherwise normally applied.

While the cut on $\not\!\!E_T$ reduces its total contribution, top quark pair production, where each top quark decays into a leptonic final state ($t \to Wb \to \ell\nu_\ell b$), may appear in our final selection, especially in our heavy-flavor tagged region. We estimate $t\bar{t}$ contributions using PYTHIA with $\sigma_{t\bar{t}} = 7.5$ pb and $m_t = 172.5$ GeV/c^2. Finally, our ZW and ZZ signal samples are also estimated using PYTHIA. The predicted and observed numbers of events are shown in Tab. I.

	All Events	Heavy Flavor-Tag Channel	Light Flavor-Tag Channel	Untagged Channel
Z + jets	$8\,667 \pm 1\,113$	93 ± 14	$1\,454 \pm 307$	$6\,721 \pm 968$
Z + b jets	714 ± 299	111 ± 48	53.8 ± 25.5	536 ± 230
$t\bar{t}$	9.2 ± 0.9	3.3 ± 0.4	0.7 ± 0.1	5.2 ± 0.6
Misidentified Leptons	330 ± 165	4.8 ± 2.4	39.4 ± 20.3	283 ± 142
Predicted Background	$9\,720 \pm 1\,247$	212 ± 55	$1,617 \pm 325$	$7\,890 \pm 1\,071$
$ZW + ZZ$	313 ± 29	12.8 ± 1.6	84.8 ± 12.3	205 ± 22
Total Predicted Events	$10\,033 \pm 1\,259$	225 ± 55	$1\,706 \pm 331$	$8\,102 \pm 1\,080$
Data Events	9 846	172	1 724	7 950

TABLE I. Predicted and observed number of events in the event selection. The uncertainties represent all systematic uncertainties, summarized in Tab. V, and in addition include a 10% uncertainty on the normalization of Z+ jets events, and a 6% uncertainty on the normalization of $ZW + ZZ$ events.

IV. JET ENERGY CALIBRATION

The jets used in this analysis have their energies, as measured by the calorimeter, corrected for a number of effects that distort the true jet energy. These effects include consistency across $|\eta|$ and time, contributions from multiple $p\bar{p}$ interactions per beam crossing (pileup) and the underlying event, the non-linear response of the calorimeter, and energy radiated outside of the jet cone. The jet energy scale (JES) corrections applied are described in detail in Ref. [17].

These energy corrections, however, do not distinguish between the response of gluon and quark jets. The largest energy corrections, which correct the energy scale of calorimeter jets to better match that of particle jets and the initial parton energies, are derived using PYTHIA [15] dijet Monte Carlo simulations. Differences in the response of gluon and quark jets between MC and data may lead to differences in the measured energies of these objects that are not covered by the previously assigned systematic uncertainties on the JES. We apply additional corrections to the energies of quark and gluon jets in simulation, as described by [18], and described in greater detail in [19].

V. ARTIFICIAL NEURAL-NETWORK QUARK/GLUON DISCRIMINANT

In this analysis, we search for two high-p_T leptons from the decay of a Z boson and two jets from a $W \to q\bar{q}'$ or $Z \to q\bar{q}$ decay; thus, the two jets in our signal are quark jets. Our dominant background, two jets produced in association with a $Z \to \ell^+\ell^-$ decay, contain a significant number of gluon jets. Separating quark jets from gluon jets will help increase our sensitivity to ZW/ZZ.

For a given energy, gluon jets, due to their higher color charge, tend to contain a higher particle multiplicity and be spatially broader in the detector than light quark (u, d, and s) jets. We attempt to quantize the spatial spread of jets using a collection of artificial neural-networks (NNs), trained to separate gluon jets from light-flavor quark jets. We call the result of the final NN the jet quark/gluon value (or jet QG value). We calibrate the response of the final NN in MC to agree with the response in data using a $W \to \ell\nu+$ 1 jet sample, and determine a tagging efficiency and mistag rate of placing a cut on the jet QG value using two independent samples: $W \to \ell\nu+2$ jets, which is similar to our $Z+$ jets

background, and $t\bar{t} \to b\bar{b}\ell\nu q\bar{q}'$, which contains two jets from the hadronic decay of a W boson, akin to our signal.

A. Jet QG Definition

A total of three NNs make up the final QG discriminant. Two networks separate quark and gluon jets by looking at the distribution of energy contained in calorimeter towers and the distribution of momenta contained in reconstructed charged-particle tracks, described in the following paragraphs. Thus, every jet may be assigned a Tower NN value and Track NN value, the output of these two NNs. These two NN values are combined in a third NN, along with other variables that offer some discrimination between quark and gluon jets, or that are related to how spread or collimated jet it is.

Each of the NNs is trained using a simulated sample of jets matched to a light flavor quark or gluon with $p_T > 20$ GeV/c and within $\Delta R = 0.4$ of the center of the jet and with no other partons above 8 GeV/c within $\Delta R = 0.7$. These jets are selected from a $Z \to \mu^+\mu^- + 2$ parton ALPGEN sample, interfaced with PYTHIA showering. Each NN is a feed-forward multilayer perceptron with a single output utilizing a tanh response function, implemented using the MLP algorithm from the TMVA package [20]. The networks are trained on 100 000 quark and gluon jets and tested for biases in over-training on a sample with 500 000 quark and gluon jets. Gluon jets are reweighted to match the E_T and η distributions of the quark jets, to remove any discrimination power coming solely from these variables.

For every jet, we obtain a list of the calorimeter towers in a cone of $\Delta R = 0.7$ around that jet. Each tower has a location coordinate, (η, ϕ), and deposited energy E associated with it. Then, for each jet, we construct a distribution of the distance, ΔR, between all pairs of towers within the jet. We weight each tower pair by its relevance in terms of energy and obtain a distribution that characterizes the spatial spread of the energy within each jet. The weight we apply to each tower pair is given by

$$\frac{E_i E_j}{0.5((\Sigma E)^2 - \Sigma E^2)} \ ,$$

where E_i and E_j are the energies of the two towers in the pair, ΣE is the sum of the energy in all towers in a cone of $\Delta R = 0.7$ around the jet, and ΣE^2 is the sum of the square of the

energy of each tower in that same cone. This denominator is chosen in order to normalize the sum of all weights of tower pairs to unity. We split this distribution into 56 bins with bin size $\Delta R = 0.025$ for $0.0 \leq \Delta R \leq 1.4$, where the contents of the first 3 bins are empty due to the segmentation of the calorimeter. Typical distributions of ΔR between tower pairs for quark and gluon jets, with a larger bin size, are shown in Fig. 1. The output of the Tower NN for quark and gluon jets in the training and testing sample is shown in Fig. 2.

We follow a similar prescription using tracks within a cone of $\Delta R = 0.7$ around each jet, using the tracks' locations in (η, ϕ) (at the primary vertex) and momenta p to obtain a distribution of the distance between pairs of tracks (in ΔR), with each pair weighted by the momentum contained within that pair, or

$$\frac{p_i p_j}{0.5((\Sigma p)^2 - \Sigma p^2)} \ ,$$

where p_i and p_j are the magnitude of the momenta of the two tracks in the pair, Σp is the scalar sum of the momenta in all tracks in a cone of $\Delta R = 0.7$ around the jet, and Σp^2 is the sum of the square of the momenta of each track in that same cone. We require all tracks within the cone around the jet come from the primary vertex, and that the track $p_T > 0.4$ GeV/c. We split the ΔR between track pairs distribution into the same 56 bins as used in the Tower NN, and the content of each bin is used as an input into the Track NN. Typical ΔR between track pairs distributions for quark and gluon jets are shown in Fig. 1. The output of the Track NN for quark and gluon jets in the training and testing sample is shown in Fig. 2.

The final NN uses the tower and track NN values as inputs, along with other jet variables that provide some discrimination power between quark jets and gluons — the ratio of ΣE in a cone of $\Delta R = 0.4$ to ΣE in a cone of $\Delta R = 0.7$, the ratio of Σp in a cone of $\Delta R = 0.4$ to Σp in a cone of $\Delta R = 0.7$, the number of towers in cones of $\Delta R = 0.4$ and 0.7, the number of tracks in cones of $\Delta R = 0.4$ and 0.7, and the jet EM fraction — and other variables that may affect the shape of the ΔR distributions, independent of whether the jet originates from a quark or gluon — the jet E_T, the jet η, and the number of reconstructed interaction vertices in the event. The output of this final ANN is shown in Fig. 3 for light-flavor quark and gluon jets from the training and testing sample.

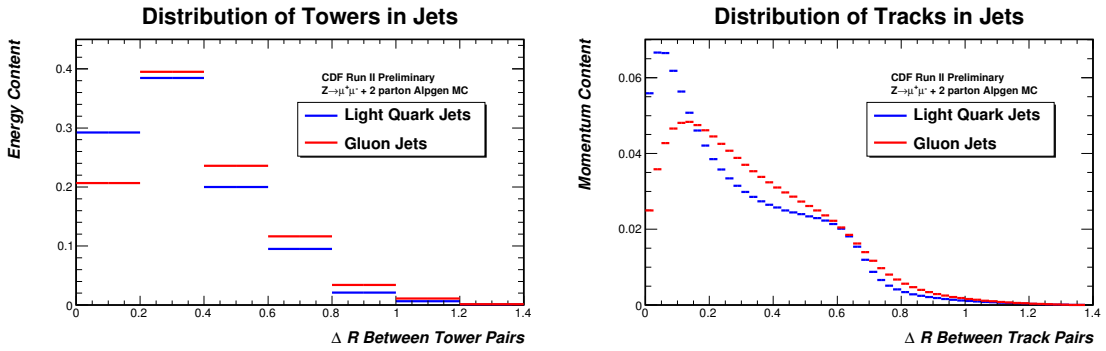

FIG. 1. Typical distributions of ΔR between pairs of towers (*left*) and between pairs of tracks (*right*) in light-flavor quark (*blue*) and gluon (*red*) jets. Light-flavor quark jets tend to peak at low ΔR, indicating they are rather collimated, while gluon jets tend to have a higher ΔR distribution. The contents of bins of these ΔR distributions are used as inputs into ANNs that discriminate between quark and gluon jets.

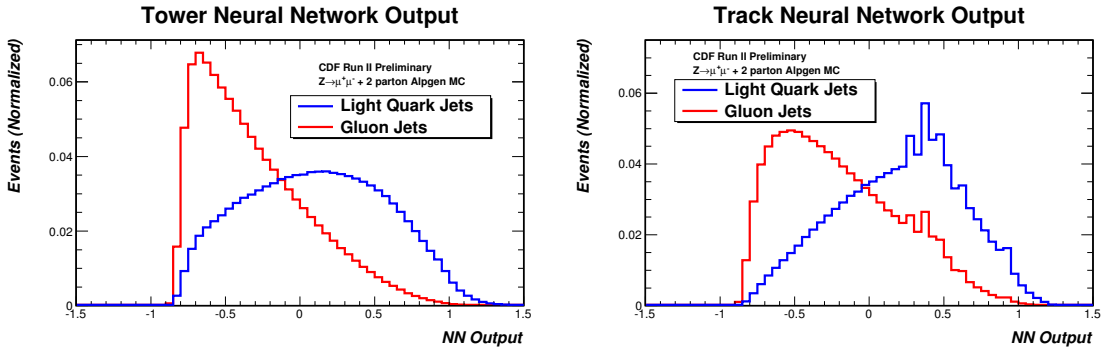

FIG. 2. The outputs of the NNs processing tower (*left*) and track (*right*) distributions in light-flavor quark (*blue*) and gluon (*red*) jets. Higher NN scores indicate jets that are more quark-like. We see good performance in both the tower and track NNs. The spiky behavior in the track NN distribution comes from jets with only two tracks located inside a cone of $\Delta R = 0.7$, and thus have only one non-zero bin in their ΔR between track pairs distribution.

B. Jet QG Calibration and Cut Efficiency/Mistag Rate

The response of the ANN quark/gluon discriminant may differ between data and MC simulation, especially since uncorrected tower energies are used in the construction of the tower NN, as we do not employ individual tower energy corrections. Since our signal and

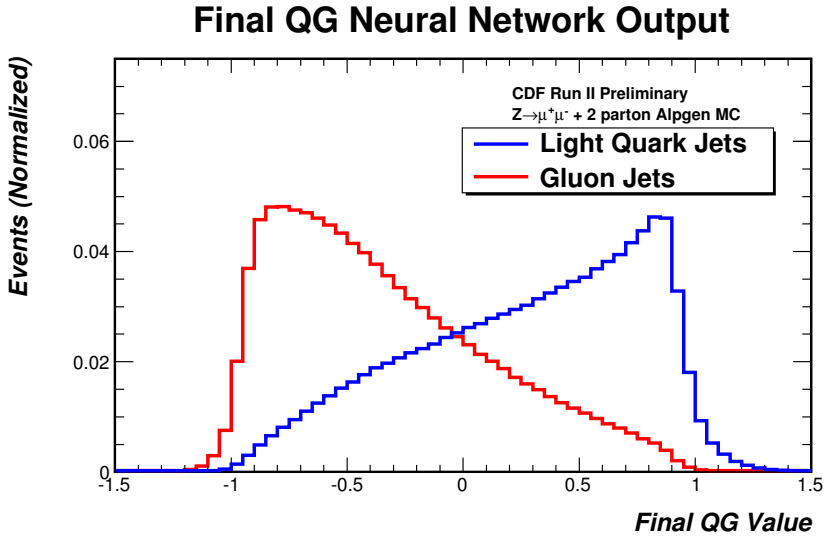

FIG. 3. The output of the final ANN for light-flavor quark (*blue*) and gluon (*red*) jets. Higher NN scores indicate jets that are more quark-like. In MC jets, we see good separation between quark and gluon jets using this discriminant.

most backgrounds are modeled with simulated data, it is necessary to calibrate the simulation response to match the behavior of the data. We do so using an independent control region with jets similar to those in our final state, $W \to \ell\nu+$ 1 jet events, and then validate the calibration and establish uncertainties on the modeling using data regions very similar to our signal and dominant background regions: $t\bar{t}$ decays in lepton + jets final states, and $W \to \ell\nu + 2$ jet events, respectively.

To form our $W + 1$ jet calibration sample, we choose data collected with the standard high-E_T/p_T central electron/muon triggers and selecting events with exactly one central ($|\eta| < 1.0$) lepton of high quality with $E_T/p_T > 20$ GeV/c. To select events consistent with a $W \to \ell\nu$ decay, we also require a large amount of missing transverse energy, $\not\!\!E_T >$ 25 GeV, and a reconstructed transverse mass [21] consistent with leptonic W decays, $m_T >$ 25 GeV/c^2. To further eliminate any contributions from multijet events where a jet mimics our lepton $+\not\!\!E_T$ signature, we require that the $\not\!\!E_T$ not be aligned with any reconstructed jet ($\Delta\phi(\not\!\!E_T$,jet) > 0.2 radians), and that the $\not\!\!E_T$-significance (as defined in [5]) be larger than 1 for events with muons, and larger than 4 for events with electrons. We require that the events in this calibration sample have exactly one jet with $E_T > 20$ GeV and $|\eta| \leq 2.0$.

We consider a number of processes that may contribute to this selection, and model them with a combination of PYTHIA, ALPGEN, and MADGRAPH [22] event generators interfaced with PYTHIA for showering. The dominant contribution is $W \to \ell\nu$ production in association with one jet, which we model using ALGPEN. As we are largely concerned with the agreement in shapes between data and simulation, we scale the simulation to match the normalization of the data. Additionally, we reweight the simulation to match the jet E_T and η distribution of the data, to remove these variables as a factor in any mismodeling of the other quantities used in forming the jet QG value.

We see poor modeling in the Tower NN values, where the jets in data appear more gluon-like than the simulated jets. That jets in data appear more spatially spread than jets in simulation is consistent with the disagreements between data and simulation in jet energies, described in Sec. IV: the amount of energy contained within a cone of $\Delta R = 0.4$ is higher in simulated gluon jets than those in data. We correct for these discrepancies using a linear shift in the Tower NN values in simulation in order to match the data in the $W + 1$ jet sample. We perform different linear shifts for jets in the central and plug calorimeters, and for jets in events with different levels of pileup. After making these calibrations in the simulated Tower NN values, we make further corrections to the response of the final NN to better match the correlations of these calibrated Tower NN values with other jet quantities: the number of towers in the jets, and the ratio of ΣE in a cone of $\Delta R = 0.4$ to ΣE in a cone of $\Delta R = 0.7$. We see better modeling in the Track NN than in the Tower NN, though we still introduce a similar linear shift in simulated Track NN values to better match data. The calibrated variables are input directly into the final NN, without retraining the network.

We further validate the response of the jet QG value by comparing data and MC simulation in $W \to \ell\nu + 2$ jets sample and in a sample of $t\bar{t}$ where two quark jets originate from the hadronic decay of a W boson. Table II summarizes the cuts placed to form these two samples: the $W + 2$ jet sample is similar to the previously described $W + 1$ jet sample, except we modify the cuts on the jets to match those used in the signal region of our $ZW/ZZ \to \ell\ell jj$ search. The $t\bar{t}$ selection eschews the $\not\!\!E_T$-sig and m_T cuts, used to reduce multijet backgrounds, in favor of requiring a minimum scalar sum of the E_T of identified objects (jets, $\not\!\!E_T$, and the lepton p_T) in the event, which is effective at removing both multijet and $W+$ jets backgrounds. Because we are interested in selecting the two jets in the $t\bar{t}$ selection that come from the decay of a W, and are not b-jets from a $t \to Wb$ decay, we

make use of the jet *b*ness tagger [23]. We classify the two jets with the highest *b*ness score as the two *b*-jets, and the remaining two jets as those resulting from a $W \to q\bar{q}'$ decay.

W + Jets Selection	$t\bar{t}$ Selection
central e or μ, $p_T > 20$ GeV/c	
$\not\!\!E_T > 25$ GeV	
$\Delta\phi(\not\!\!E_T$,Nearest Jet) > 0.4 rad	$\Delta\phi(\not\!\!E_T$,Nearest Jet) > 0.2 rad
$\not\!\!E_T$-sig > 4 (e only)	
$W m_T > 25$ GeV/c^2(e only)	
	Sum $E_T > 300$ GeV
$N_{jets}(E_T > 20$ GeV$) = 2$	$N_{jets}(E_T > 20$ GeV$) = 4$
	2^{nd} highest *b*ness jet > -0.5
$1^{\text{st}}/2^{\text{nd}}$ jet $E_T > 25$ GeV	2 highest *b*ness jets $E_T > 20$ GeV
	2 lowest *b*ness jets $E_T > 25$ GeV
Jets' $\lvert\eta\rvert < 2.0$	
ΔR between jets > 0.7	

TABLE II. Summary of event selection requirements for our $t\bar{t}$ lepton + jets selection and our W + 2 jets selection, used to understand the modeling of events in our QG discriminant. Cuts in the center are shared cuts in the two samples.

Because we are looking for jet QG shape differences between data and simulation that will translate to acceptance uncertainties when we place a cut on the jet QG value, we scale the number of $W+$ jet events in simulation to match the data in our $W+2$ jets sample. The number of events in each sample is shown in Tab. III. The distributions of the maximum and minimum QG values of the two jets considered are shown in Fig. 4. We see fairly good modeling in the $t\bar{t}$ sample, but poorer modeling in the $W + 2$ jet sample, where, after our calibrations, the jets in simulation appear more gluon-like than the jets in data.

We find maximum sensitivity to our signal when forming a "light-flavor tagged" channel by requiring the minimum jet QG value of the jets in our analysis be > 0.0. We determine an efficiency for quarks to pass this cut, and gluons to be "mistagged" using this cut, with

	W + jets Selection	$t\bar{t}$ Selection
W + jets[a]	21520 ± 2150	38.7 ± 3.9
$W + b$ jets[a]	937 ± 375	13.8 ± 5.5
Z/DY + jets	1249 ± 125	3.1 ± 0.3
Z/DY + b jets	86 ± 34	1.4 ± 0.6
WW/WZ	1386 ± 83	5.9 ± 0.4
single t	767 ± 77	19.6 ± 2.0
$t\bar{t}$	1378 ± 83	469 ± 28
$t\bar{t}$ (b-jets)		108 ± 7
$t\bar{t}$ (q-jets)		361 ± 22
Total Expected	27319[a]	551 ± 30
Data	27319	579

[a] $W+$ jets samples have been scaled to as to produce agreement with data in the number of events.

TABLE III. The number of events in the W + 2 jets and $t\bar{t}$ lepton + jets region, showing only the uncertainties assigned on the normalization of each sample. The distinction between b and q jets in the $t\bar{t}$ sample refers to the lower two $b$ness jets: events where both jets are matched to non-b quark jets are labeled "q-jets", while if one of the jets is matched to a b jet, it is labeled "b-jets".

the $t\bar{t}$ and $W + 2$ jet samples. The efficiency measured in data, $e_D(q)$, as it is a function of the QG cut placed, may be expressed as

$$e_D(q) = \frac{e_{raw}(q) - s_m(q) m_{MC}(q) f_g}{1 - f_g} \ , \tag{1}$$

where e_{raw} is the fraction of data events passing the QG cut; m_{MC} is the mistag rate for gluons to pass the cut, as measured in simulation; s_m is a scale factor on the mistag rate in simulated jets to match the mistag rate measured in data; and f_g is the fraction of gluon jets in the sample. We can write a similar expression for getting the mistag rate from

$$m_D(q) = \frac{m_{raw}(q) - s_e(q) e_{MC}(q) f_q}{1 - f_q} \ , \tag{2}$$

where m_{raw} is the fraction of data events passing the QG cut; e_{MC} is the efficiency for quarks

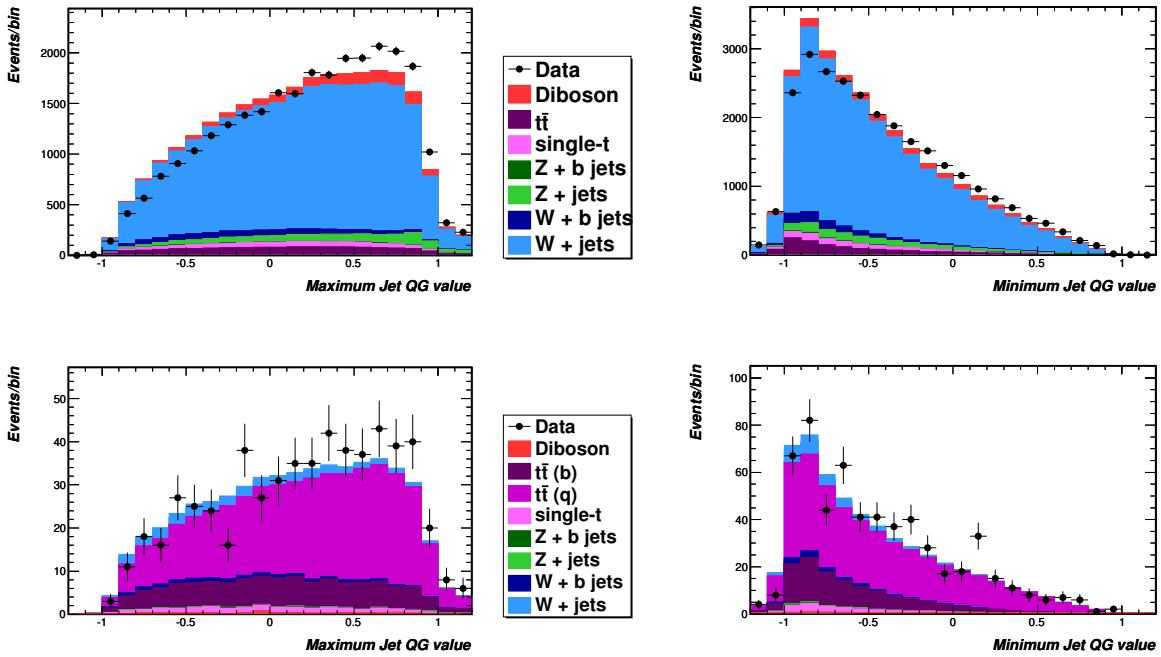

FIG. 4. Distribution of the maximum (*left*) and minimum (*right*) jet QG values of the two jets in our $W + 2$ jet (*top*) and $t\bar{t}$ (*bottom*) samples. The distinction between b and q jets in the $t\bar{t}$ sample refers to the lower two $b$ness jets: events where both jets are matched to non-b quark jets are labeled "q-jets", while if one of the jets is matched to a b jet, it is labeled "b-jets".

to pass the cut, as measured in simulation; s_e is a scale factor on the efficiency in simulated jets to match the mistag rate measured in data; and f_q is the fraction of quark jets in the sample. Uncertainties on these quantiites may be expressed as

$$\begin{aligned}\sigma_e^2(q) = \frac{1}{(1-f_g)^2}\left(\frac{e_{\rm raw}(1-e_{\rm raw})}{N_D} + (\sigma_m f_g)^2\right) \\ + \sum_X \frac{\sigma_X^2}{\left[N_{\rm MC}(1-f_g)\right]^2} \times \\ \left[(e+s_m m)(f_g - f_g^X) + f_q^X(e_{\rm MC} - e_X)\right]^2 \ , \end{aligned} \tag{3}$$

where N_D and N_{MC} are the number of data and simulated events, and where the X represents the various subsamples of the simulation. A similar expression may be written for the mistag rate. The uncertainty here includes a statistical uncertainty on the data, uncertainties on the mistag rate and efficiency, and uncertainties on the relative difference in the contributions

from the simulation. We take the uncertainties on the normalizations of our $t\bar{t}$, single-t, diboson, W/Z + jets, and $W/Z + b$ jets to be 6%, 10%, 6%, 10%, and 40%, respectively.

We measure the efficiency in the $t\bar{t}$ sample, where we have a very small number of gluon jets, and measure the mistag rate in the $W + 2$ jets sample, where the gluon fraction is much larger and similar to our $Z + 2$ jet signal region. The efficiency and mistag rate and their uncertainties are determined using an iterative procedure, as they rely on one-another. We first calculate the mistag rate in data first assuming the efficiency in data is equivalent to that in simulation. We then calculate the efficiency in data assuming that mistag rate, and proceed to recalculate the mistag rate assuming the new efficiency from data. We see rapid convergence on the final measurements of the efficiency and mistag rate. Table IV shows the efficiency and mistag rate for our given cut at minimum QG > 0.0, measured in both data and MC. We see that the MC underestimates the rate for quark jets to pass the jet QG cut, while correctly predicting the observed mistag rate.

	MC	Data	MC Eq. Cut (-1σ,Nom.,$+1\sigma$)
Efficiency	0.241	0.295 ± 0.034	$(-0.0325, -0.09, -0.14)$
Mistag Rate	0.088	0.087 ± 0.027	$(0.09, -0.0175, -0.11)$

TABLE IV. The efficiency and mistag rates for our QG cuts, as evaluated in data and MC, along with the necessary cut value changes in MC to model the proper rates and the uncertainties on them.

We implement a correction to the MC by shifting the cut on the minimum QG value in order to match the efficiency/mistag rate of the data. The uncertainties on these quantities are also implemented using this shift in cut, allowing us to have both rate and shape uncertainties due to the QG tag requirement. The shifted cut values used for MC quark and gluon jets are listed in Tab. IV.

VI. SIGNAL EXTRACTION AND RESULTS

We extract the number of signal events using a binned χ^2-minimization fit to data, using methods described in Ref. [24]. We supply histogram templates for our signal and background samples. The templates, along with the uncertainties we assign to their normalization in the fit procedure, are listed below:

- ZW/ZZ signal: We allow the normalization of the signal template to float unconstrained in the fit. We assume each signal process contributes proportionally to its predicted SM cross section: 3.6 pb for ZW and 1.5 pb for ZZ [1].

- Z + jets: This is our largest background, and we also allow its normalization to float in the fit, unconstrained.

- $Z + b$ jets: A significant background in the b-tagged channel, we constrain this template's normalization within $\pm 40\%$.

- $t\bar{t}$: We assign an uncertainty of 6.5%, based on the theoretical cross section uncertainty [25], on the normalization of this template.

- Misidentified Leptons: We use the method described in Sec. III to construct templates for the contribution from jets mimicking one or two leptons. We assign an uncertainty of 50% on the misidentification rate, based on studies using different trigger thresholds in the jet data used to obtain these rates.

We perform a simultaneous fit to data using these templates in three channels. For events passing the basic signal selection requirements described in Sec. III, we first construct a heavy-flavor tag (HF-tag) channel composed of events passing a minimum jet $b$ness requirement (jet $b$ness > 0), using the jet $b$ness tagger [23]. For events failing this requirement, we then pick events passing the minimum jet QG value requirement described in Sec. V to form a light-flavor tag (LF-tag) channel. Events failing this requirement are then placed in the third "untagged" channel, which has a lower signal fraction than the two tagged channels, but still has a significant amount of signal due to the tight placement of the tagging requirements.

Additional systematic uncertainties on both the normalization and shapes of the templates used in the fit are also considered. We consider uncertainties due to mismodeling

Systematics in Fit	Channel	WZ and ZZ	Z + jets	$Z + b$ jets	$t\bar{t}$	Misidentified Leptons
σ/Norm.	all	*unconstr.*	*unconstr.*	±40%	±6.5%	±50%
Jet Resolution	HF-Tag	±0.8%	±0.3%	±1.0%	±0.2%	
	LF-Tag	±1.0%	±0.7%	±1.5%	±6.2%	
	No-Tag	±0.6%	±0.9%	±0.7%	±1.1%	
Jet Energy Scale	HF-Tag	±4.0%	±4.4%	±3.8%	±4.0%	
	LF-Tag	±1.5%	±0.3%	±0.6%	±3.0%	
	No-Tag	±1.9%	±5.7%	±3.8%	1.9%	
Q^2	all		shape only	shape only		
ISR/FSR	all	shape only				
*b*ness Tag	HF-Tag	±7.8%	±7.8%	±9.2%	±7.6%	
	LF-Tag	±0.2%	±0.0%	±1.2%	±2.8%	
	No-Tag	±0.4%	±0.1%	±1.8%	±4.5%	
QG Tag	LF-Tag	±10%	±16%	±2.0%	±15%	
	No-Tag	±4.3%	±3.5%	±2.0%	±2.0%	
Lepton Energy Scale	all	±0.5%	±0.5%	±0.5%	±1.5%	
Lepton Energy Res.	all	±0.1%	±0.1%	±0.0%	±2.7%	

TABLE V. Summary of the systematic uncertainties considered in the fit of the dijet mass distribution. Uncertainties that change both the shape and rate of templates used in the fit are treated in a correlated fashion.

between data and MC simulation in the jet energy scale (as described in Sec. **??**) and the jet energy resolution, the modeling of the tagging variables, and the lepton energy scale and resolution. Additional shape uncertainties on the Z + jets backgrounds are considered by varying the renormalization and factorization scale, Q^2, up and down by a factor of two. We also consider the effect on the shape of the dijet invariant mass when increasing or decreasing initial and final state radiation in our ZW/ZZ signal. These systematic uncertainties, along with the normalization constraints described above, are treated as nuisance parameters in the fit, and included in the χ^2-minimization procedure [24] and are summarized in Tab. V.

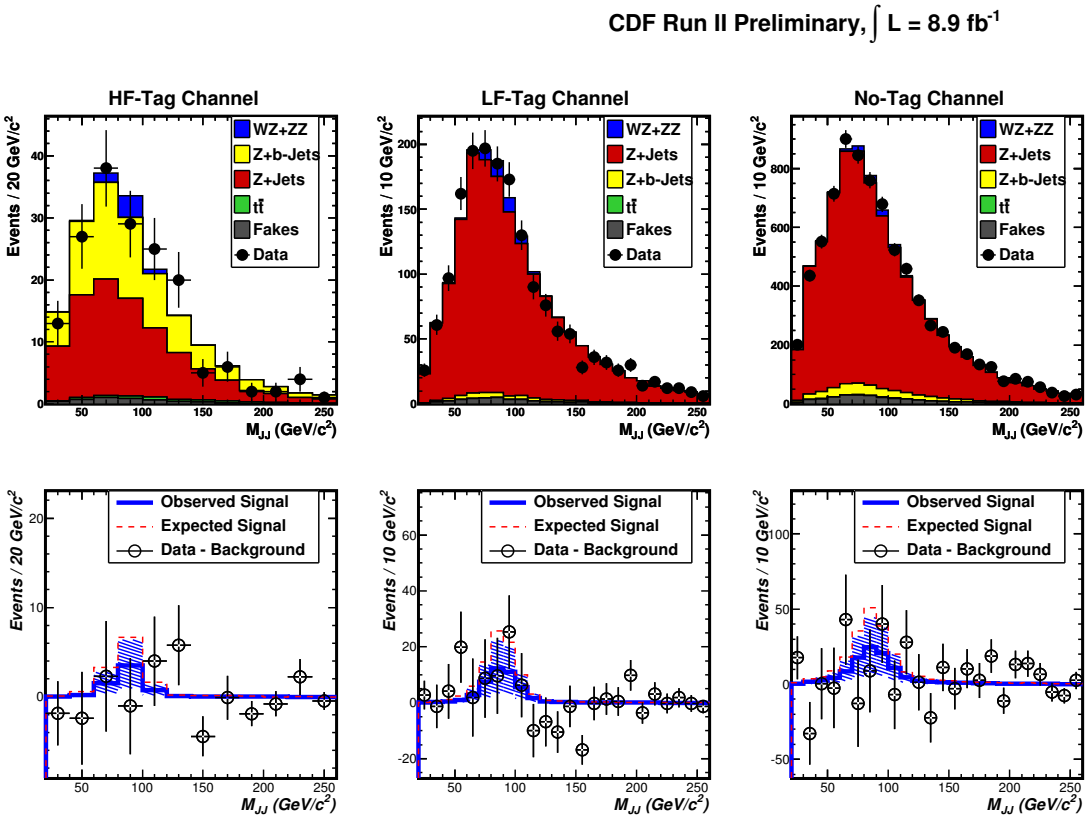

FIG. 5. Result of the fit to data for ZW/ZZ in our dilepton + dijet selection in our HF-tag channel (*left*), HF-tag channel (*center*), and untagged channel (*right*). The top row shows the output from the fit compared to the data, while the bottom row shows the background subtracted from data, compared to the expected (*red dashed line*) and fitted (*blue solid line, with uncertainties in blue bands*) signal contributions.

Figure 5 shows the result of the fit to signal, and we show the number of events fit for in each template in Tab. VI. We fit for $\approx 50\%$ of the expected signal normalization, and see good agreement between data and simulation in the final fit in each of the three fitting channels, with a total χ^2/d.o.f= 59.8/55.

We establish bounds and limits on the cross section of ZW/ZZ production using a Feldman-Cousins method [26], where we analyze the distribution of measured cross sections in pseudo-experiments generated with a variety of scale factors on the input signal cross section. When generating pseudo-experiments, we consider additional systematic uncertainties that affect our acceptance, assigning a 2% uncertainty from parton distribution functions to the signal template, and 2.5% and 6% uncertainties on all templates derived

Process	N_{events}, HF-Tag	N_{events}, LF-Tag	N_{events}, No-Tag
Z + jets	91.9 ± 8.3	1605 ± 50	7200 ± 600
$Z + b$ jets	71 ± 14	37 ± 10	360 ± 100
$t\bar{t}$	3.18 ± 0.35	0.71 ± 0.07	5.26 ± 0.42
Fakes	4.6 ± 2.3	39 ± 20	270 ± 140
Total Bkg.	171 ± 14	1681 ± 36	7840 ± 600
$ZW + ZZ$	6.3 ± 4.4	45 ± 30	106 ± 72
Total Events	177 ± 14	1726 ± 40	7940 ± 610
Data Events	172	1724	7950

TABLE VI. The number of events in each fitting channel from our best fit to the data.

from simulation due to the lepton scale factor determination and luminosity, respectively. The set of input cross sections in our pseudo-experiments range from 0.0 to 2.9 times the expected cross section, with a step size of 0.1.

Figure 6 shows the results of our Feldman-Cousins analysis. Using the 1σ bands, we measure $\sigma(p\overline{p} \rightarrow ZW/ZZ) = 2.5^{+2.0}_{-1.0}$ pb, compared to the standard model prediction of $\sigma_{SM} = 5.1$ pb. We do not exclude the no-signal hypothesis, and establish a limit of $\sigma_{ZW/ZZ} <$ 6.1 pb ($1.25 \times \sigma_{SM}$) at the 95% C.L.

VII. HIGH DIJET p_T REGION

We perform an additional study of the dijet mass spectrum using a set of cuts meant to mimic those used in a study of the invariant mass distribution of jet pairs produced in association with a leptonically decaying W boson [7]. In addition to the selection requirements described in Sec. III, we require the reconstructed dijet p_T to be greater than 40 GeV/c and the two leading jets to have $E_T > 30$ GeV. We also remove events with a third jet whose E_T is greater than 30 GeV. The number of predicted and observed events is shown in Tab. VII.

For this set of cuts, we do not split our final selection sample into three orthogonal fitting channels; instead, we leave all events passing the selection in one channel. Also, we constrain the diboson cross section to be within 6% of the predicted cross section. The result of the

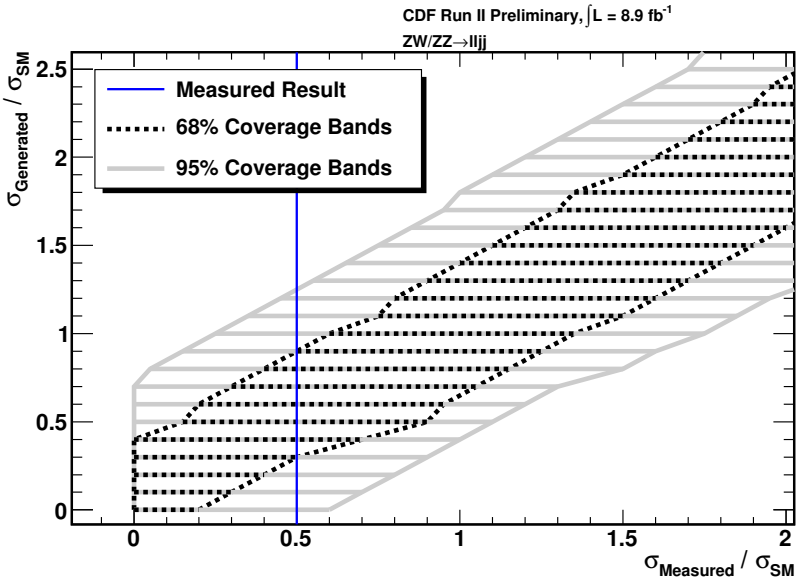

FIG. 6. Condence bands showing the expected range of measured cross sections as a function of the true cross section, with 68% CL (black dashed region) and 95% CL (solid gray region). Our measured result of $\sigma(p\overline{p} \rightarrow ZW/ZZ) = 2.5^{+2.0}_{-1.0}$ pb corresponds to a limit of $\sigma_{ZW/ZZ} < 6.1$ pb $(1.2 \times \sigma_{SM})$ at the 95% C.L.

	Events
Z + jets	$3\,016 \pm 382$
$Z + b$ jets	267 ± 111
$t\bar{t}$	4.8 ± 0.5
Misidentified Leptons	102 ± 51
Diboson $(ZW + ZZ)$	129 ± 13
Total Predicted Events	$3\,517 \pm 430$
Data Events	3 349

TABLE VII. Predicted and observed number of events in the event selection with increased jet thresholds and dijet p_T. The uncertainties represent the same systematic uncertainties as described in Sec. VI, and in addition include a 10% uncertainty on the normalization of Z+ jets events, and a 6% uncertainty on the normalization of $ZW + ZZ$ events.

fit is shown in Fig. 7. We see good agreement between data and simulation in this fit, with

χ^2/d.o.f= 23.9/22. The inclusion of an extra, Gaussian-shaped signal centered around 145 GeV/c^2 – similar to that proposed in [7] – does not improve the fit.

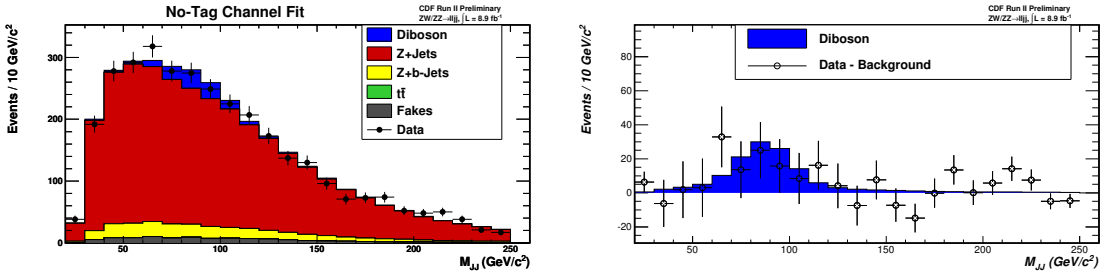

FIG. 7. Result of the fit to data for ZW/ZZ in our dilepton + dijet selection in a selection with high dijet p_T and increased jet energy thresholds. On the left is the result of the fit, and on the right is the fit with all components, excepting the diboson, subtracted. We see the fit to the data is good, and we see no significant excess around 145 GeV/c^2.

VIII. CONCLUSIONS

We describe a search for ZW/ZZ diboson production in a final state with two charged, high-E/p_T electorns/muons and two hadronic jets at the CDF detector. We take events from a suite of high-E/p_T lepton triggers, increasing our acceptance to diboson production over using only single-lepton triggers. We increase our sensitivity by tagging jets likely coming from heavy and light flavor quarks, and placing them in their own fitting channels. These NN-based taggers benefit from the large sample of top quarks produced at CDF, allowing us to derive a data-driven estimate of the efficiency and mistag rates for jets passing our tagging requirements. We also improve the modeling of our Monte Carlo simulations, especially those that describe our $Z+$ jets background, by deriving and incorporating new jet energy corrections to jets to better match the behavior of quark and gluon jets in data.

Using data over the entirety of CDF Run II, an integrated luminosity of 8.9 fb^{-1}, we fit for the normalization of $ZW/ZZ \to \ell^+\ell^- + q\bar{q}'$ events using the dijet invariant mass distribution. We incorporate many of the systematic uncertainties in this analysis as parameters in the dijet mass fit. While we expected a measurement of $\sigma_{ZW+ZZ} = 5.1 \pm 2.0$ pb, corresponding to a significance of about 2.6σ, we measured a cross section of $\sigma_{ZW+ZZ} = 2.5^{+2.0}_{-1.0}$ pb. This result is significant at about 1.75σ. We also report a limit on the cross section: $\sigma_{ZW+ZZ} <$

6.1 pb at 95% CL. This measurement is consistent with the Standard Model prediction.

ACKNOWLEDGMENTS

We thank the Fermilab staff and the technical staffs of the participating institutions for their vital contributions. This work was supported by the U.S. Department of Energy and National Science Foundation; the Italian Istituto Nazionale di Fisica Nucleare; the Ministry of Education, Culture, Sports, Science and Technology of Japan; the Natural Sciences and Engineering Research Council of Canada; the National Science Council of the Republic of China; the Swiss National Science Foundation; the A.P. Sloan Foundation; the Bundesministerium für Bildung und Forschung, Germany; the Korean World Class University Program, the National Research Foundation of Korea; the Science and Technology Facilities Council and the Royal Society, UK; the Russian Foundation for Basic Research; the Ministerio de Ciencia e Innovación, and Programa Consolider-Ingenio 2010, Spain; the Slovak R&D Agency; the Academy of Finland; the Australian Research Council (ARC); and the EU community Marie Curie Fellowship contract 302103.

[1] J. M. Campbell and R. K. Ellis, Phys. Rev. D **60**, 113006 (1999).

[2] K. Hagiwara *et al.*, Nucl. Phys. **B 282**, 253 (1987).

[3] M. Kober, B. Koch, and M. Bleicher, Phys. Rev. D **76**, 125001 (2007).

[4] E. J. Eichten, K. Lane, and A. Martin, Phys. Rev. Lett. **106**, 251803 (2011).

[5] T. Aaltonen *et al.* (CDF Collaboration), Phys. Rev. Lett. **103**, 091803 (2009).

[6] T. Aaltonen *et al.* (CDF Collaboration), Phys. Rev. Lett. **104**, 101801 (2010).

[7] T. Aaltonen *et al.* (CDF Collaboration), Phys. Rev. Lett. **106**, 171801 (2011).

[8] V. M. Abazov *et al.* (D0 Collaboration), Phys. Rev. Lett. **108**, 181803 (2012).

[9] T. Aaltonen *et al.* (CDF Collaboration), Phys. Rev. D **85**, 012002 (2012).

[10] A. Abulencia *et al.* (CDF Collaboration), J. Phys. G **34**, 2457 (2007).

[11] The coordinate system used to describe the detector has its origin located at the detector's center. The proton beam direction is defined as the $+z$ direction. The polar angle, θ, is measured from the origin with respect to the z axis, and ϕ is the azimuthal angle. Pseudorapidity, transverse energy, and transverse momentum are defined as $\eta{=}-\ln\tan(\theta/2)$, $E_T{=}E\sin\theta$, and $p_T{=}p\sin\theta$, respectively. The rectangular coordinates x and y point radially outward and vertically upward from the Tevatron ring, respectively.

[12] F. Abe *et al.* (CDF Collaboration), Phys. Rev. D **45**, 1448 (1992).

[13] We define the missing transverse momentum $\vec{\not\!\!E}_T \equiv -\sum_i E^i_{\rm T}\mathbf{n}_i$, where $\mathbf{n}_i$ is the unit vector in the azimuthal plane that points from the beamline to the ith calorimeter tower. We call the magnitude of this vector $\not\!\!E_T$.

[14] M. L. Mangano *et al.*, J. High Energy Phys. **07**, 001 (2003).

[15] T. Sjöstrand *et al.*, J. High Energy Phys. **05**, 026 (2006).

[16] T. Aaltonen *et al.* (CDF Collaboration), Phys. Rev. D **79**, 052008 (2009).

[17] A. Bhatti *et al.*, Nucl. Instrum. Methods A **566**, 375 (2006).

[18] CDF Public Note **10973** (2013).

[19] W. R. Ketchum, FERMILAB-THESIS-2012-36.

[20] A. Hoecker, P. Speckmayer, J. Stelzer, J. Therhaag, E. von Toerne, and H. Voss, PoS **ACAT**, 040 (2007), arXiv:physics/0703039.

[21] We define the transverse mass as $m_T = \sqrt{2p_T^{\text{lepton}} \not\!\!E_T \left(1 - \cos\Delta\phi_{\ell,\not\!\!E_T}\right)}$, where $\Delta\phi_{\ell,\not\!\!E_T}$ is the difference in ϕ in the direction of the lepton $\vec{p_T}$ and $\vec{\not\!\!E}_T$ vectors.

[22] J. Alwall *et al.*, J. High Energy Phys. **09**, 028 (2007).

[23] J. Freeman *et al.*, Nucl. Instrum. Methods A **663**, 37 (2012).

[24] T. Aaltonen *et al.* (CDF Collaboration), Phys. Rev. D **82**, 112005 (2010).

[25] U. Langenfeld, S. Moch, and P. Uwer, Phys. Rev. D **80**, 054009 (2009).

[26] G. J. Feldman and R. D. Cousins, Phys. Rev. D **57**, 3873 (1998).